Title
HIGH TEMPERATURE FAILURE MECHANISMS IN CERAMIC POLYCRYSTALS

Authors
Evans, A.G.
Blumenthal, W.

Publication Date
1983-12-01

Lawrence Berkeley Laboratory
UNIVERSITY OF CALIFORNIA

Materials & Molecular Research Division

To be presented at the Second International Conference on Creep and Fracture of Engineering Materials and Structures, Swansea, Wales, United Kingdom, April 1-6, 1984

HIGH TEMPERATURE FAILURE MECHANISMS IN CERAMIC POLYCRYSTALS

A.G. Evans and W. Blumenthal

December 1983

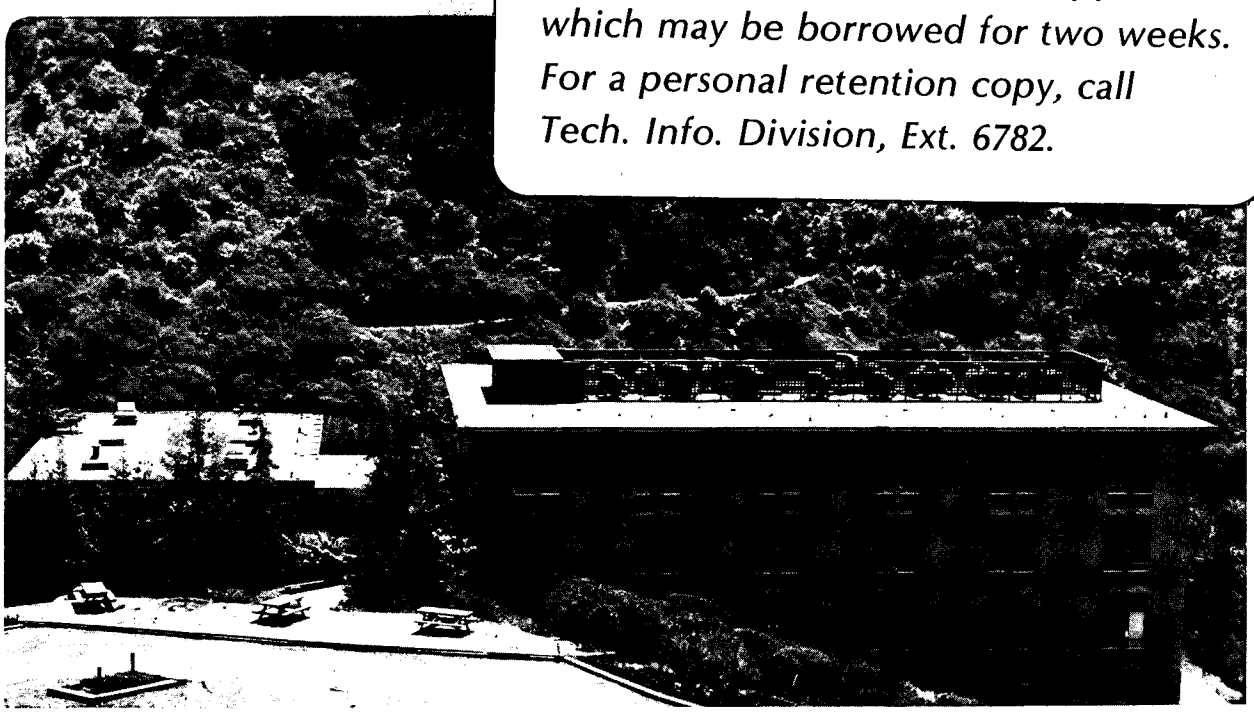

Prepared for the U.S. Department of Energy under Contract DE-AC03-76SF00098

DISCLAIMER

HIGH TEMPERATURE FAILURE MECHANISMS IN CERAMIC POLYCRYSTALS

A. G. Evans, and W. Blumenthal

Materials and Molecular Research Division,
Lawrence Berkeley Lab., Dept. of Materials Science and
Mineral Engineering, Univ. of Calif., Berkeley, CA 94720

ABSTRACT

The high temperature failure of ceramics has been observed to occur by the nucleation, growth and coalescence of cracks. Each process involves diffusive cavity nucleation and growth, either within a damage zone or at microstructural heterogeneities. The specific cavitation and cracking mechanisms pertinent to ceramics are described and available models are presented. Particular emphasis is placed on continuous crack nucleation at microstructural heterogeneities and the crack coalescence process that causes eventual failure. Failure time data are also reviewed and correlated with models.

1. INTRODUCTION

The high temperature failure of fine grained polycrystalline ceramics generally occurs by the nucleation, growth and coalescence of cracks, as illustrated by the sequence depicted in Fig. 1. The limiting stage of failure depends on the material, temperature and environment. Each stage requires thorough investigation, in order to derive a generic model of creep rupture pertinent to ceramic polycrystals. Some progress toward this objective has been realized, but a complete model is not yet available. This article describes the present status of understanding, as well as the phenomena that require further investigation before an adequate failure model can be developed.

2. GENERAL CHARACTERISTICS

Observations performed on ceramic materials reveal [1] (Fig. 1a) that cracks typically nucleate, at microstructural heterogeneities, well before eventual failure. However, the original cracks usually blunt [2] (Fig. 1b) and new cracks nucleate continuously throughout the failure process.

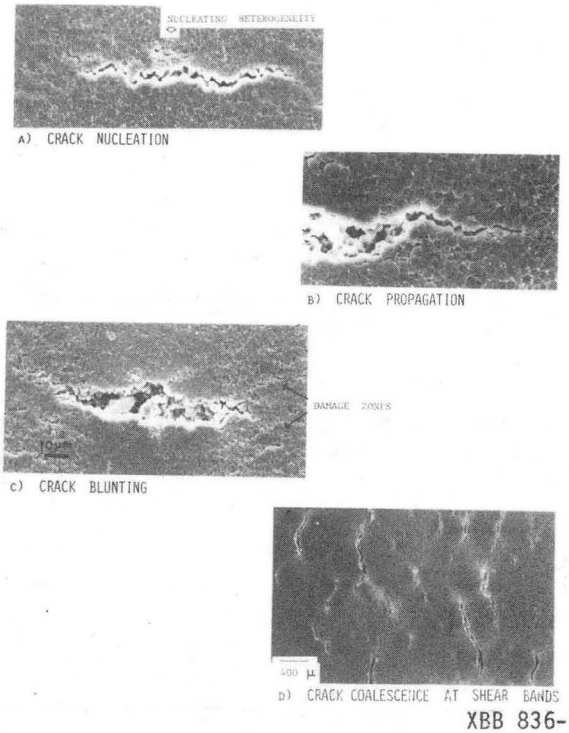

XBB 836-5001A

Fig. 1. Scanning electron micrograph of Al_2O_3 specimens illustrating the various stages of failure (a) crack nucleation at heterogeneities (b) crack propagation (c) crack blunting (d) crack coalescence.

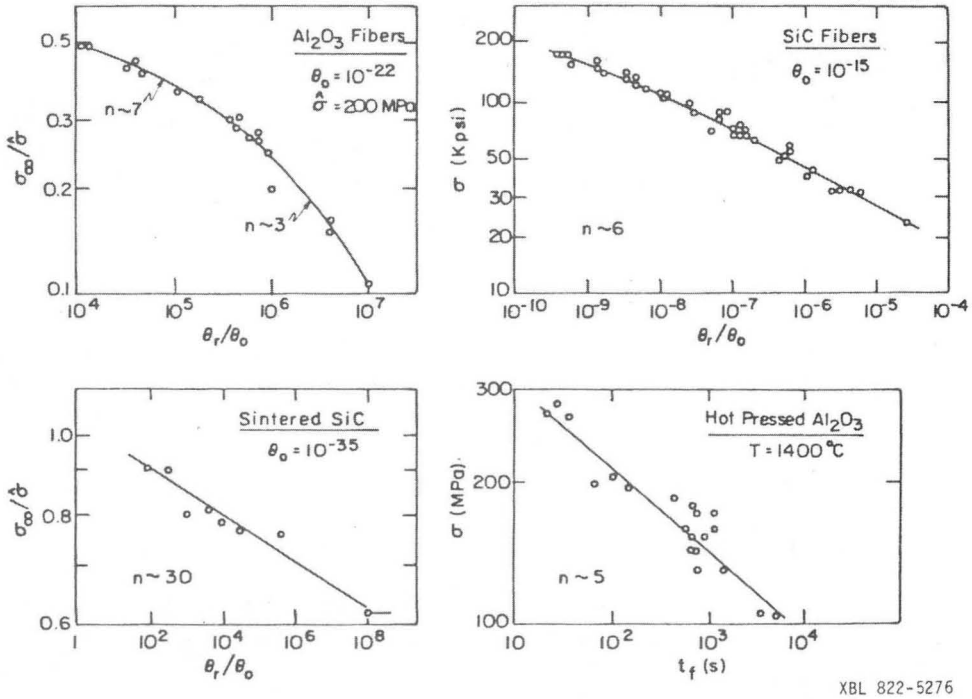

XBL 822-5276

Fig. 2. Relationships between failure time and stress for ceramic polycrystals.

Creep-related failure appears to involve the coalesence of blunted cracks, along shear bands between crack tips (Fig. 1d) [3]. Consequently, the processes of continuous nucleation, growth, blunting and coalescence of creep cracks all require study.

The measured relationships between failure time and stress for most ceramics are highly non-linear [3-6] (Fig. 2). For example, recent data obtained on "single phase" alumina [3] indicate that the failure time, t_f, varies with stress, σ, as;

$$t_f \dot{\varepsilon}_\infty = (\sigma_o / \sigma)^6 \qquad (1)$$

where $\dot{\varepsilon}_\infty$ is the remote strain-rate and σ_o is a constant. The specific source of the non-linearity is not yet evident. The eventual objective of research studies on high temperature failure is to provide an adequate non-linear model, based on analysis of each stage in the failure process.

3. CRACK NUCLEATION

Cracks in ceramic polycrystals nucleate preferentially at microstructural and chemical heterogeneities [1,2]. The microstructural heterogeneities include large grained regions (Fig. 3a) and large single grains or inclusions, as well as delaminations (Fig. 3b). The large grains are considered to be sites for premature crack nucleation for two reasons. They act as creep inhomogeneities, which induce local stress concentrations [1], and they probably contain interfaces susceptible to cavity nucleation. Analysis of the stress concentrations that accrue, due to a viscosity differential, reveals that stresses up to about twice the applied stress are generated in and around the heterogeneity [1] (Fig. 4) until cracking occurs. This level of stress concentration is generally not large enough to account for cavity nucleation on interfaces free of second-phase. Consequently, the additional presence of precipitates or second phases that encourage nucleation, within the zones of stress concentration, are inferred. For example, large grained regions Al_2O_3 have been associated with the presence of TiO_2 [7], which may create a second phase amenable to cavity nucleation on sliding interfaces. Additional research is needed to establish a full understanding of these inhomogeneities.

The delaminations that are observed as intrinsic cracks [1] (Fig. 3b) are typical hot pressing defects. Similar crack-like entities form between agglomerates [8,9] during rapid local densification, and resist sintering. The presence of some remaining fine porosity (Fig. 3b) supports the supposition that the present defects result from incomplete local sintering.

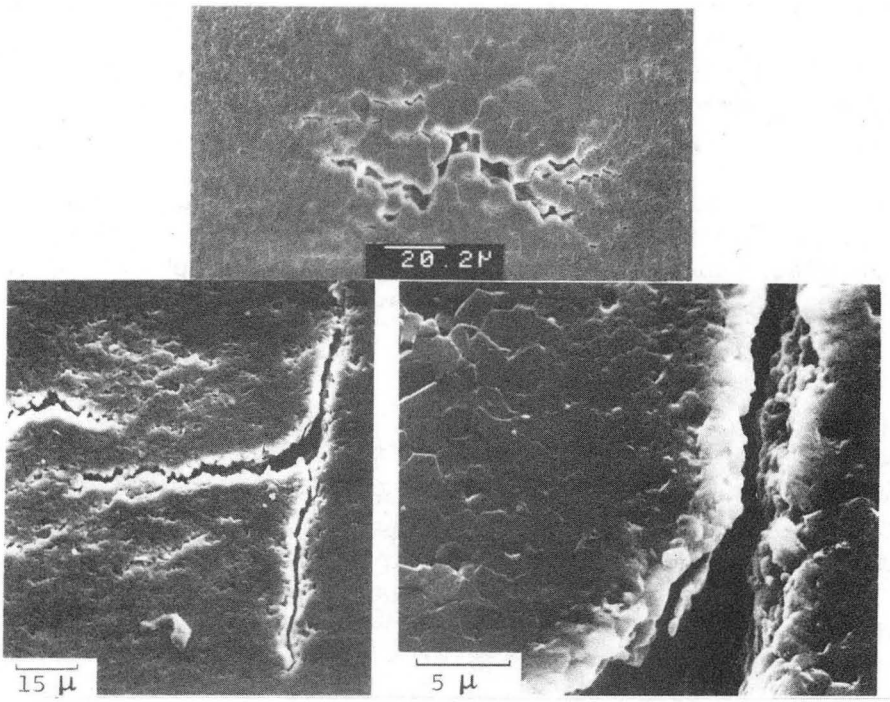

Fig. 3. Crack nucleation at microstructural heterogeneities. (a) Large grained region and (b) a delamination; note the residual fine porosity.

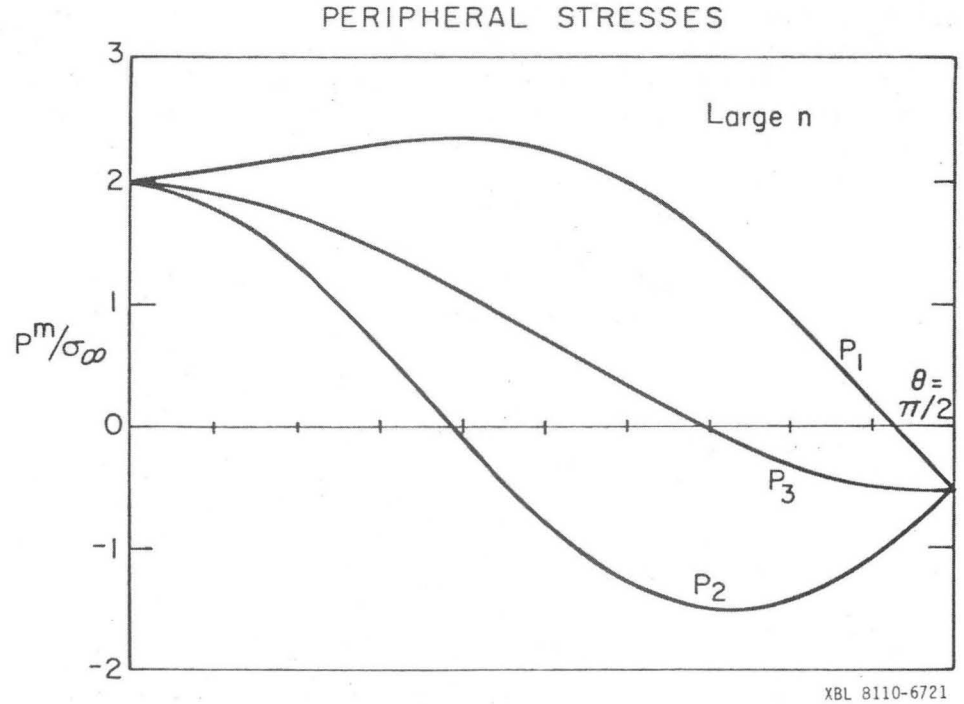

Fig. 4. The variation of stress in and around a spherical heterogeneity as a function of the relative viscosity of the matrix and the defect.

Chemical heterogeneities often consist of second phases that oxidise preferentially during the test. Typical examples are inclusions in Si_3N_4 [10,11], and regions containing excess amorphous material. Evidence for the latter heterogeneity has been obtained in Al_2O_3, and manifests as spots that thermally etch at a more rapid rate than the surrounding microstructure [1-3] (Fig. 1a).* The presence of excess Si in these regions has been used to imply the existence of an amorphous silicate phase. Profuse crack nucleation invariably occurs at such locations (Fig. 1d). Furthermore, cracks extend at a relatively rapid rate radially outward from these regions [2], as discussed in the following section.

Oxidisable regions in Si_3N_4 include areas with a high local concentration of Fe, Co and W [12] (either as precipitates or in solid solution). The preferred oxidation of these regions results in the formation of pits, containing low viscosity amorphous material. An attendant stress concentration (Fig. 5). thus obtains. Again the stress concentration presumably interacts with other local heterogeneities to nucleate cracks, as depicted in Fig. 5. However, the magnitude of the pit size needed to induce crack nucleation has not been investigated. A scale effect (similar to that which pertains for cracking due to thermal expansion mismatch [13]) is expected, but has not been verified.

4. CRACK GROWTH AND BLUNTING

4.1 Crack Growth

The growth characteristics of both induced surface cracks and intrinsically nucleated cracks have been subject to investigation [2,14]. The former have been most extensively studied and exhibit the characteristics depicted in Fig. 6a. Crack growth occurs between a threshold K_{th} and the critical stress intensity K_c. In Al_2O_3, for example, blunting occurs at $K < 0.4\ K_c$ and crack healing initiates at $K < 0.2\ K_c$. The crack growth rates are asymptotic with respect to both the threshold and critical stress intensities. The crack growth rate, a, in the intermediate range, can generally be characterized by;

$$\dot{a} = \dot{a}_o\ (K/K_c)^n\ \exp[-Q/RT] \qquad (2)$$

where n is an exponent comparable to the steady state creep exponent ($\dot{\varepsilon}_\infty \sim \sigma^n$), $\dot{a}_o$ is a constant and Q is the activation energy for steady state creep.

The growth mechanism in the intermediate range is microstructure dependent. In essentially single phase materials,

*Evidence suggests that at least some of the observed regions result from surface contamination.

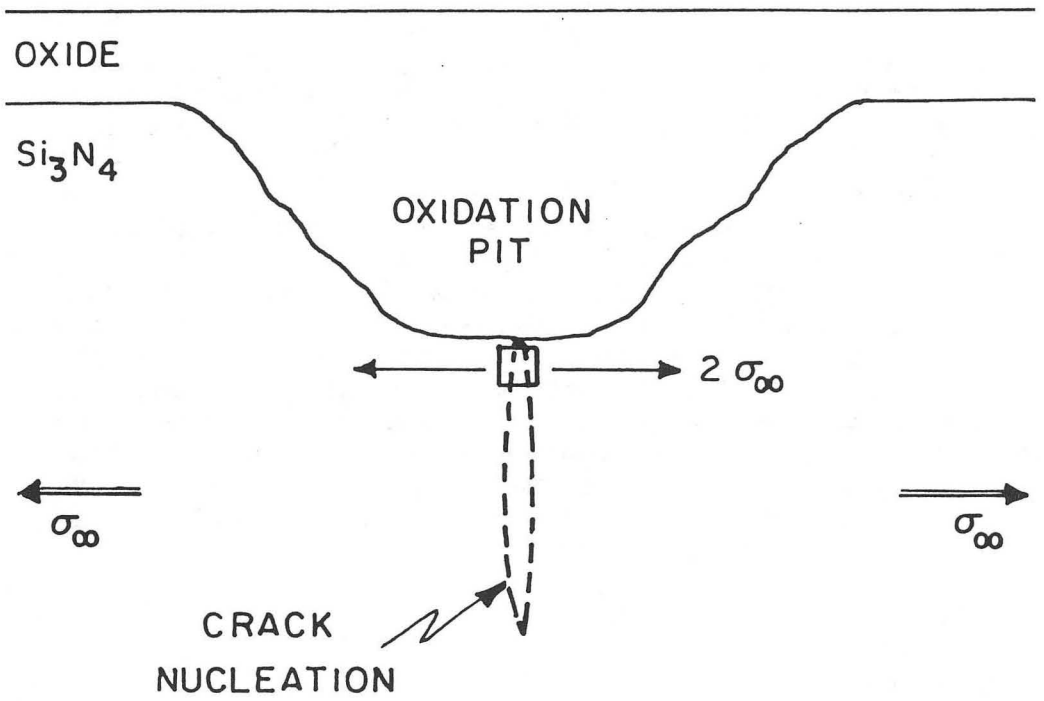

Fig. 5. A schematic illustrating the stress concentration that occurs around oxidation pits and the consequent nucleation of cracks.

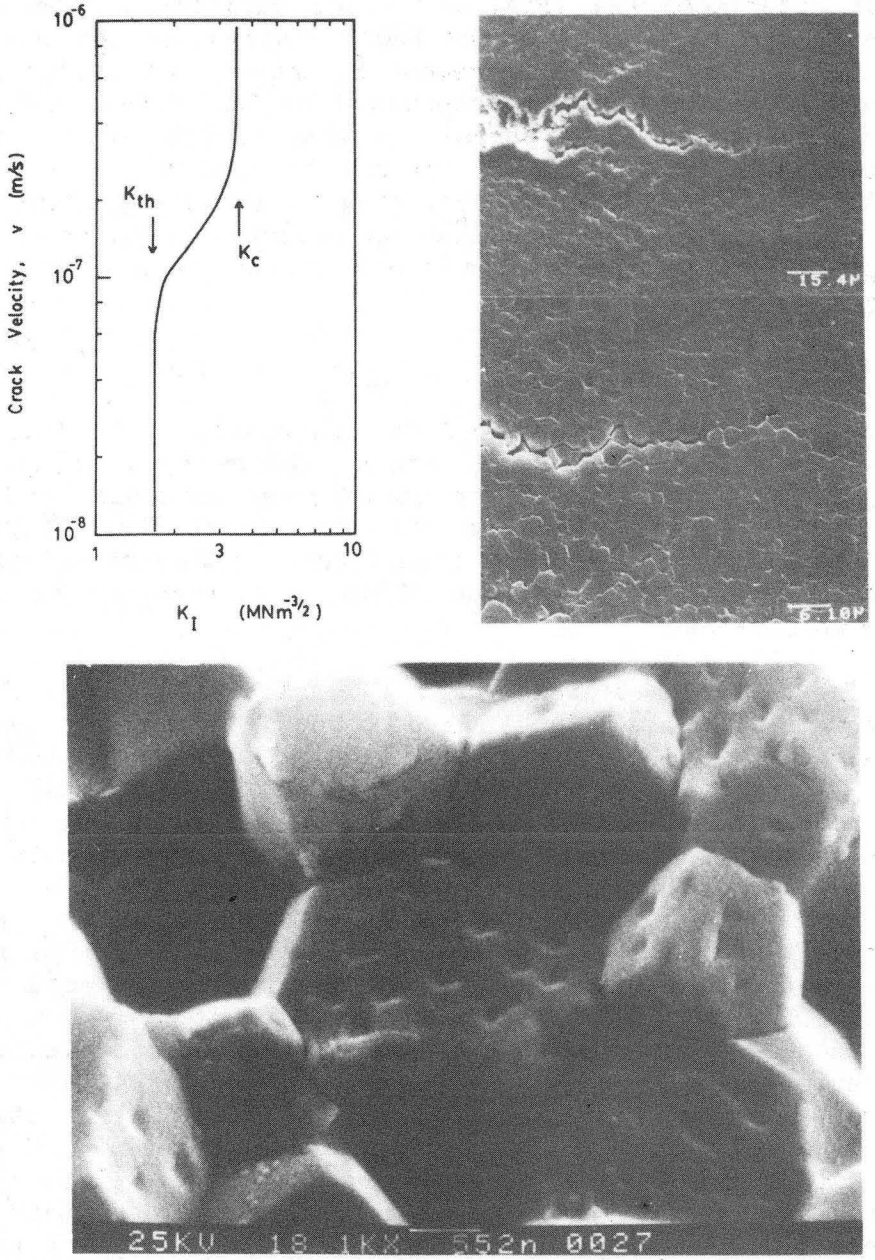

XBB 832-1354A

Fig. 6. a) A schematic of crack growth characteristics for extrinsic cracks indicating the threshold, K_{th}, the critical stress intensity, K_c, and the intervening region of creep crack growth.
b) A scanning electron micrograph of a growing crack profile, indicating coplanar damage.
c) A scanning electron micrograph of a crack growth surface revealed by brittle fracture at room temperature, showing cavities on two grain interfaces.

crack growth proceeds by the development of a small damage zone (Fig. 6a,b) consisting primarily of cavities on two grain interfaces [2] (Fig. 6a). The cavities in the damage zone grow and coalesce on the facet contiguous with the crack to permit a facet-sized increment in crack growth. The cavity growth occurs at a rate determined by the stress acting on the damage zone. This stress consists of the crack tip singular field, substantially relaxed by viscous (creep) constraint of the dilatation occurring in the damage zone [15]. The cavity spacing, λ, is also an important rate controlling quantity. Consequently, the crack growth rate has the form [15]

$$\dot{a}_\eta = K\sqrt{l}\, F(\lambda/l,\ z,\ A_f) \qquad (3)$$

where η is the viscosity of the material, l is the facet size, z is the damage zone length, A_f is the area of facet subject to cavitation at the coalescence condition and F is the function plotted in Fig. 7. The damage zone length and the coalescence area are significant determinants of the crack growth rate, by virtue of their effects on the damage zone constraint.

The result predicted by Eq. (3) coincides quite well with experimental data for Al_2O_3, when the experimentally observed λ/l is incorporated (Fig. 6c). However, as yet, there is no real understanding of the effect of microstructure on λ. Further studies of cavity nucleation are needed to address this important issue, as discussed in section 6.

In materials that contain a continuous amorphous phase, crack growth involves the nucleation of holes in the second phase within a damage zone [16]. Hole nucleation occurs predominantly at three grain pockets (Fig. 8) with growth and coalescence proceeding by coupled viscous flow and solution/reprecipitation. Because the damage zone morphology and, hence, the constraint, have not been adequately studied, models of this process are still rather qualitative. However, the parameters that influence crack growth in the single phase polycrystals must also be important in these materials, since rapid crack growth is expected to occur in materials with a low viscosity and a small hole spacing.

Intrinsically nucleated cracks are often observed to grow at more rapid rates than induced surface cracks. The growth rate differential is especially marked during initial extension of the crack out of the nucleating heterogeneity (Fig. 9a). The enhanced growth could be attributed, in part, to creep induced stress concentrations. However, local excesses of amorphous material are also of paramount importance. Amorphous material accelerates crack growth by the mechanism depicted in Fig. 9b. The amorphous phase penetrates the grain boundary by dissolving the major phase. The stress on

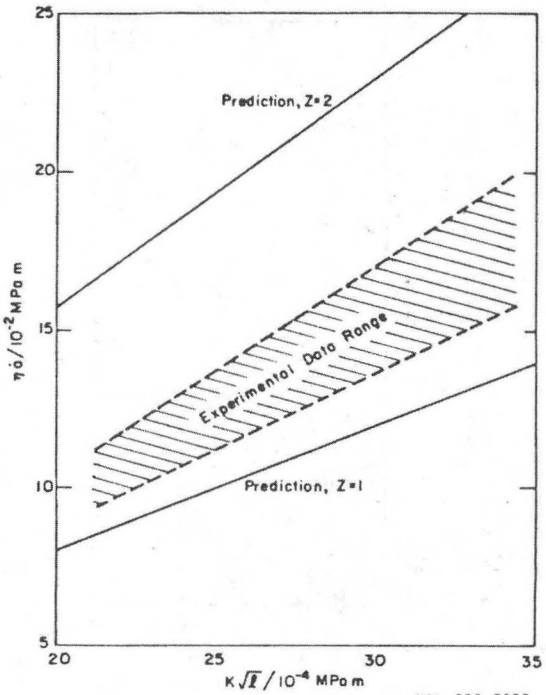

Fig. 7. The crack growth rate predicted by a coplanar damage model compared with experimental data for Al_2O_3.

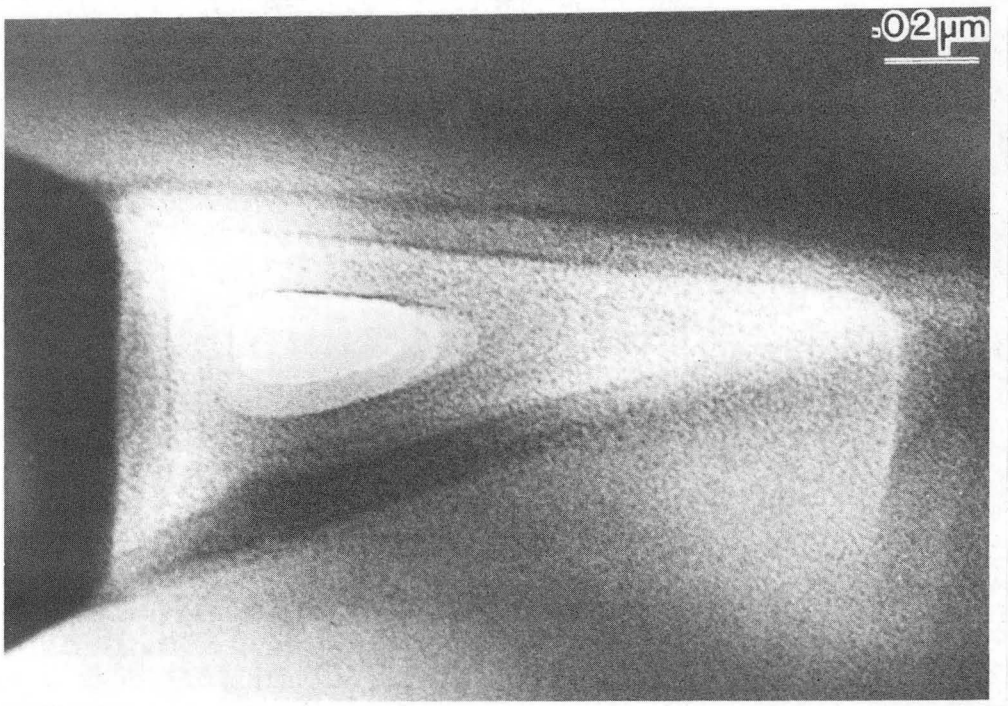

Fig. 8. Hole nucleation at an amorphous pocket in Si_3N_4.

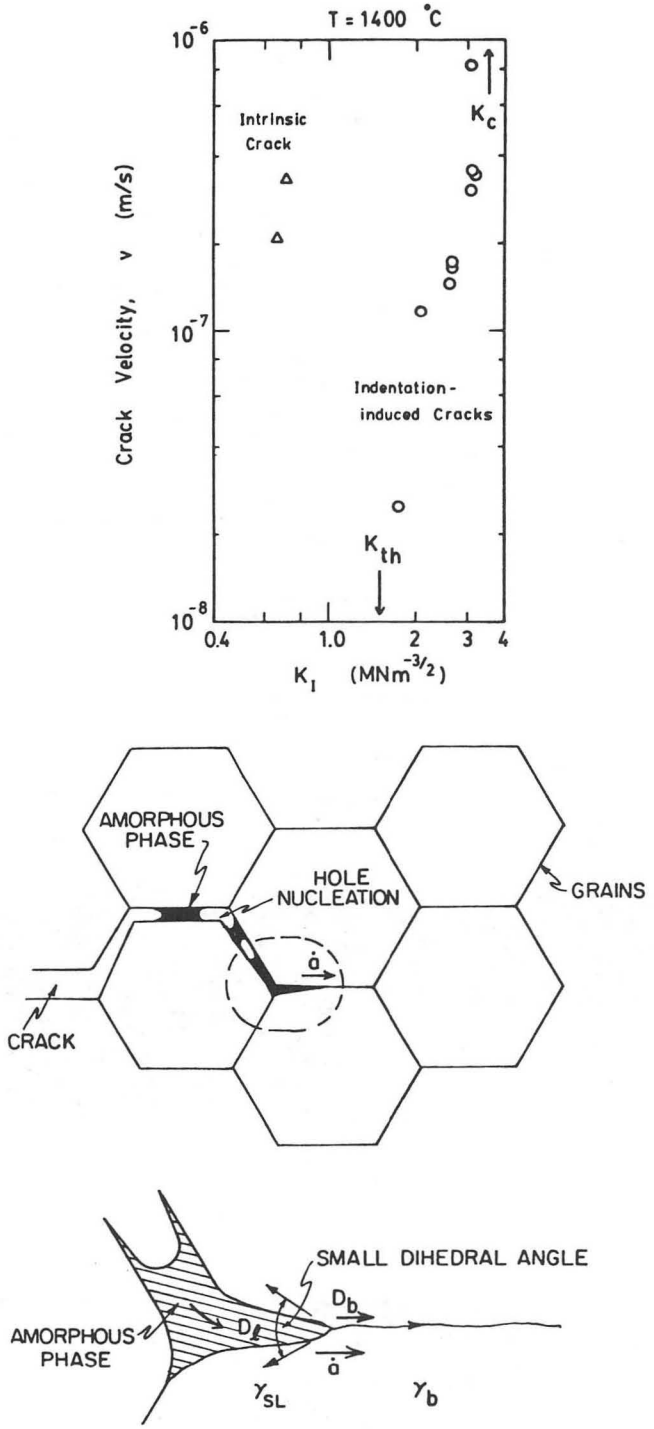

Fig. 9. The growth characteristics of intrinsically nucleated cracks. a) The growth rate for initial growth compared with that for extrinsic cracks. b) A schematic illustrating the role of an amorphous phase in the acceleration of intrinsic cracks.

the liquid then causes hole nucleation. The dissolved major phase material migrates into the grain boundary from the crack surfaces, by means of solution/precipitation process. Preliminary analysis indicates that liquid flow, dictated by the meniscus curvature, controls the rate of crack growth. Continued growth of the crack from the reservoir of amorphous material appears to eventually deplete the crack of amorphous phase and the crack then arrests and blunts, whenever $K < K_{th}$ (Fig. 10a). The eventual coalescence of these blunted cracks (Fig. 1d) results in failure.

4.2 Blunting

At stress intensities, $K < K_{th}$, the cracks blunt (Fig. 10a,b) (at least in the absence of an amorphous phase). Blunting, although exhibiting several morphologies (Fig. 10b), is invariably accompanied by a damage zone of substantial size. The damage zone consists of a high density of full-facet sized cavities (Fig. 10c) manifest as side lobes emanating from the crack tip [2]. Coalescence of the cavities within the damage zone often results in bifurcation intercepting the crack surface behind the original crack tip (Fig. 10b). The transition from frontal damage at $K > K_{th}$, to side lobe damage, at $K < K_{th}$, is clearly a major cause of crack blunting. However, the reasons for this transition are not well understood.

The damage envelope resembles the contours of maximum shear stress (Fig. 11). Infact, the damage zones are subject to both appreciable shear and tension [2]. However, normal stress in uniaxial tension is relatively constant ahead of the crack tip. Consequently, since cavity growth is motivated by the normal stress--and occurs on boundaries normal to the maximum tension (Fig. 12)--the role of the shear stress is presumed to reside in its effect either on cavity nucleation (e.g., due to grain boundary sliding transients) [17] or on enhanced creep accommodation of the dilatation in the developing damage zone [18].

5. CRACK COALESCENCE

Recent observations (Fig. 13) indicate that final failure occurs by the coalescence of blunted cracks across intervening shear bands. These shear bands, which consist of material substantially damaged by full-facet cavities (see Fig. 10c), presumably support most of the creep strain in the latter stages of failure. Shear strain concentrations between arrested cracks thus ensue and undoubtedly cause the linking of the side lobe damage between neighboring cracks. Enhanced creep then occurs in the intervening damage zone, as motivated both by the increased compliance provided by the cracks (Fig. 14) and the magnified creep rate allowed by the damage. The generation of cavities in the shear band, due to the presence

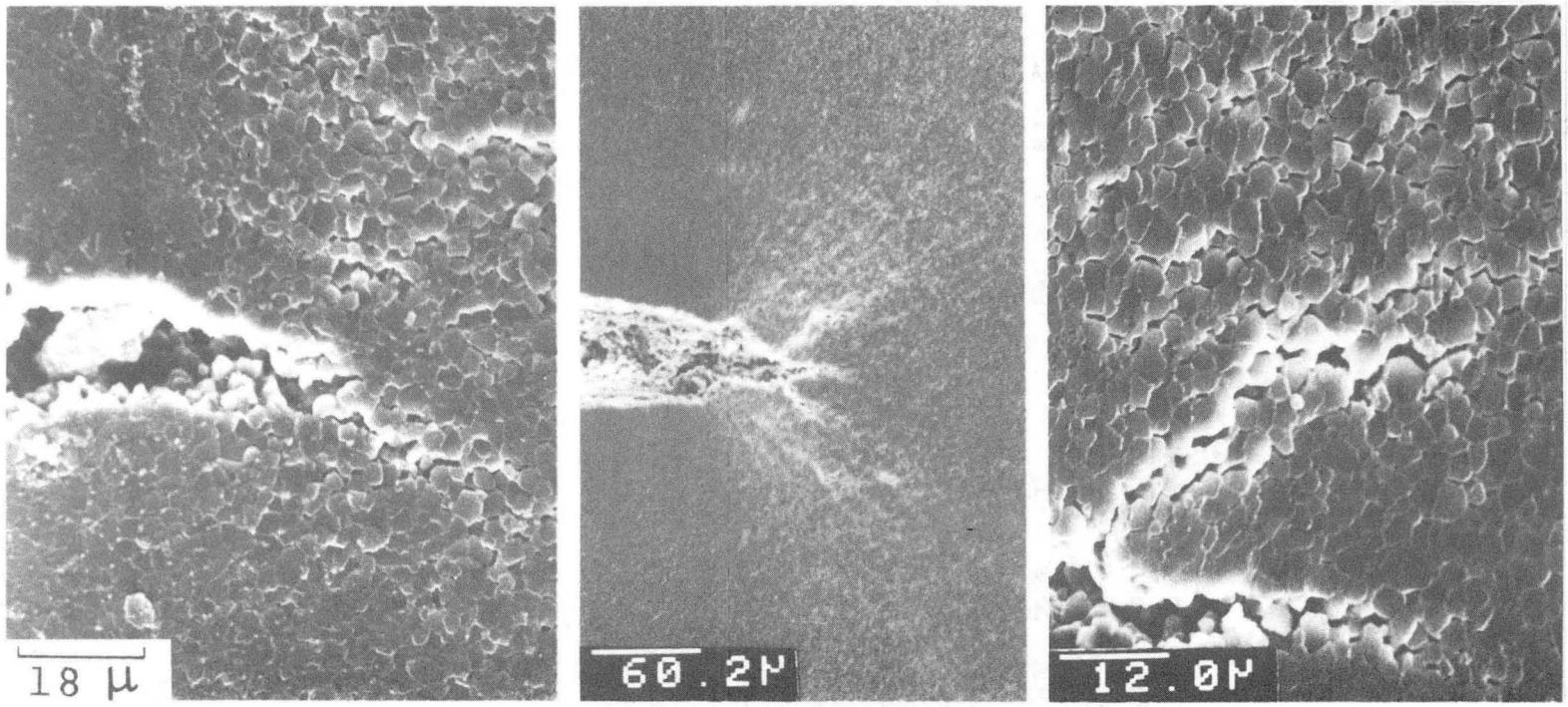

XBB 836-5990

Fig. 10. a) The blunting configuration for intrinsic cracks.
b) Blunting configuration for extrinsic cracks.
c) The cavitation damage within the side lobes of blunted cracks.

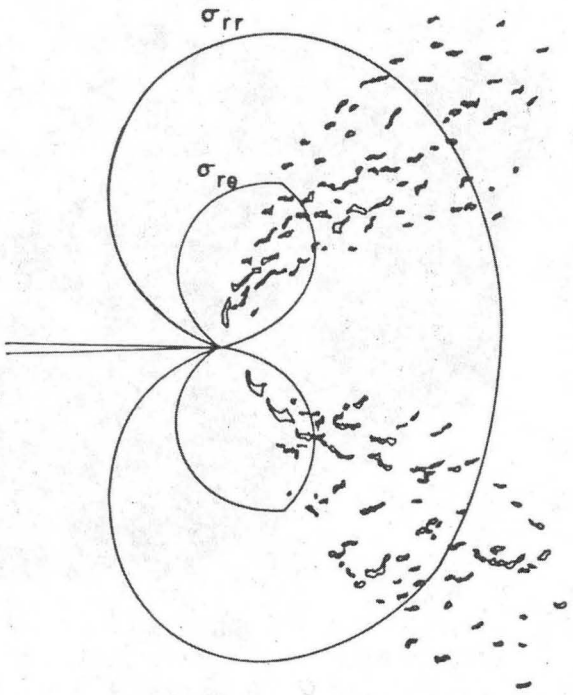

XBL 837-10644

Fig. 11. Stress contours around a crack tip compared with the damage zone contours.

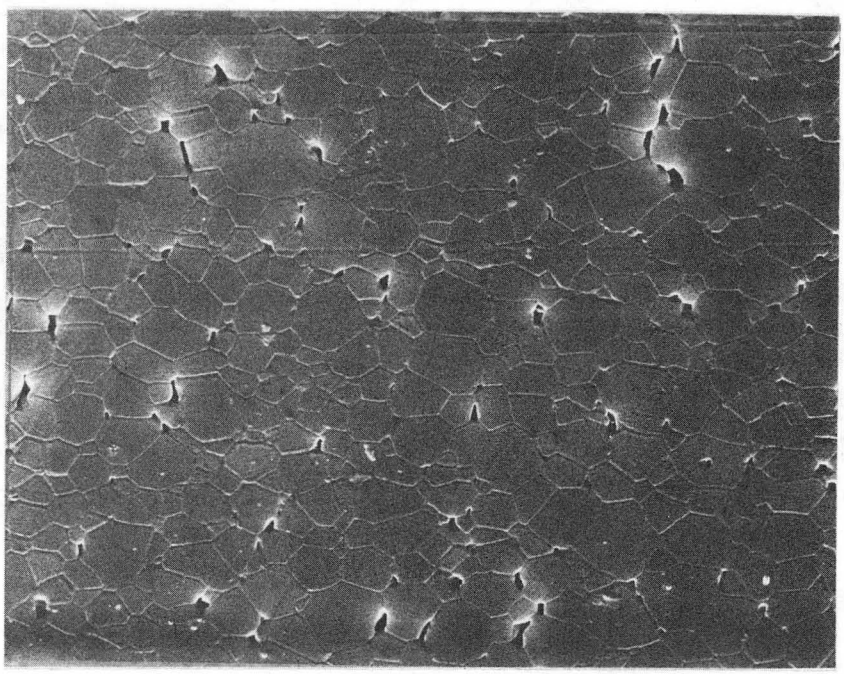

XBB 804-4499

Fig. 12. Cavitation damage in a uniaxial test growing normal to the principal tension.

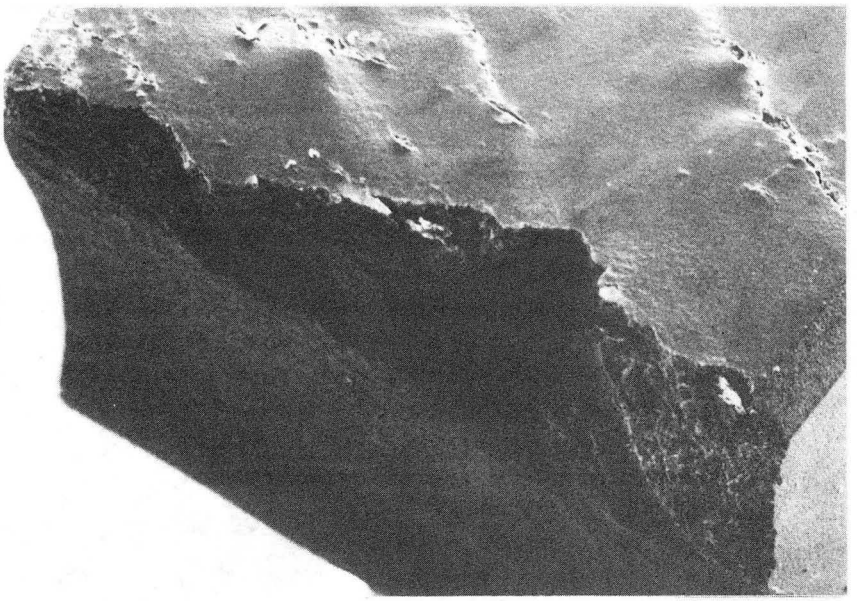

XBB 836-5002

Fig. 13. A scanning electron micrograph of a failure surface indicating that the crack has extended through the shear bands. (Courtesy Brian Dalgleish)

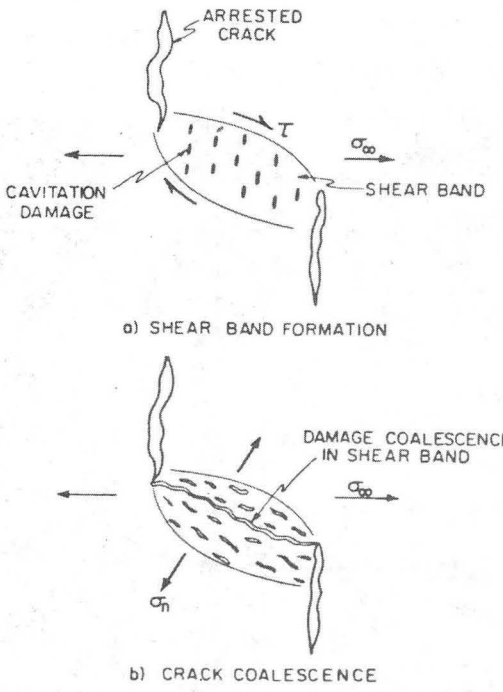

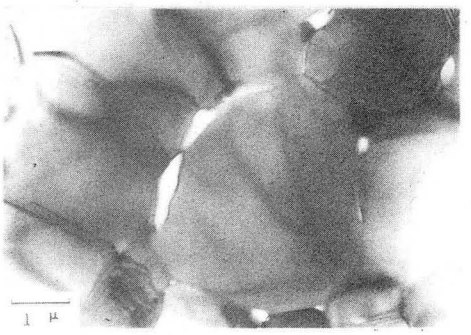

XBL 837-5985

XBB 836-5498

Fig. 14. A transmission indicating failure by cracking across shear bands.

Fig. 15. A transmission electron microscope image of material in the damage zone at the blunting threshold. (Courtesy Brian Dalgleish)

of the normal stress (Fig. 14) results in coalescence of the cavities and linkage of the crack. Continued joining of contiguous, blunting cracks eventually results in a macro crack with sufficient size that $K > K_{th}$ (Fig. 6a), whereupon macroscopic creep crack growth can occur and cause final failure (in accord with the process described in Section 4.1). This description of crack coalescence and failure, although qualitatively consistent with observations, has not yet been adequately modelled. Further discussion of various possibilities is presented in the following section.

6. DISCUSSION

6.1 The Cavity Spacing

The preceding description of high temperature failure has revealed that the spacing between cavities exerts an important influence on several stages of failure. This spacing is undoubtedly dependent on the microstructure and the mechanism of cavity nucleation. Yet, the quantitative association between microstructure and cavity nucleation have not yet been formulated. There is substantial evidence that nucleation is related to the incidence of grain boundary sliding transients [17]. This mode of cavity nucleation is supported by the present observation that the damage around cracks at the blunting threshold occurs in zones subject to the highest shear stresses. Sliding transients generate appreciable stress concentrations at triple points, non-deformable precipitates and boundary undulations. These stress concentrations undoubtedly account for sliding induced nucleation, perhaps in conjunction with local fluctuations in dihedral angle associated with precipitates and/or solutes. However, the precise requirements for nucleation are not known; albeit that most data suggest an average density of nucleation sites that increases with strain (probably because of the associated cumulative incidence of sliding transients). The cavity spacing is also subject to uncertainty, except in situations where non-deformable precipitates are the preferred nucleation sites, whereupon the precipitate spacing controls the cavity spacing. The wavelength of boundary undulations has been proposed as one possible spacing determinant, but adequate validation of this proposal has yet to be obtained. Studies of boundary structure in relation to cavity spacing are clearly of substantial importance. Cavities have also been observed to nucleate at slip band intersections with grain boundaries [19]. This process is probably of little significance in fine-grained materials which are devoid of dislocations [2] in the damage zone* (Fig. 15).

*The absence of dislocations is not necessarily construed to exclude the presence of some dislocation activity, but to negate the incidence of slip bands with stress concentrations of a sufficient spatial extent to induce stable cavities.

6.2 The Failure Time

The specific stage that dominates the failure time and its dependence on stress, temperature and microstructure has not been well studied. Hence, quantitative assessment of failure times is not presently justified. Nevertheless, useful insights can be gained by examining preliminary models of the various stages involved in failure. Such models are summarised in the Appendix and herein, their implications are cursorily reviewed.

Present comprehension suggests that failure is not dominated by either the initial crack nucleation stage or the final macrocrack propagation stage, because both processes exhibit small deviation from linearity in stress (at least when intrinsic crack nucleation precedes failure). Specifically, the nucleation of a single crack has been considered to satisfy a Monkman-Grant law, $t_f \dot{\epsilon}_\infty$ constant. While crack growth from the threshold, K_{th}, to the critical stress intensity, K_c, yields a failure time, $t_f \sim \sigma^{-2}$.

The paucity of data concerning the velocity of intrinsic cracks and their probability of nucleation prohibits evaluation of the growth of individual intrinsic cracks as a major determinent of the failure time. Consequently, the only failure stage amenable to present analysis and capable of providing adequate non-linearity is a coalescence process based on the continuous nucleation of intrinsic cracks. In this process, failure is dominated by the time taken to nucleate cracks on sufficient contiguous nucleation sites which then creates a macrocrack subject to a stress intensity $K > K_{th}$. The non-linearity in this process derives from the stress dependence of the crack nucleation probability and the macrocrack formation condition. However, adequate evaluation of this coalescence model awaits experimental data concerning the stress dependence of the intrinsic crack nucleation probability. Furthermore, the specimen size effect that necessarily obtains for this process has not been experimentally assessed.

Therefore, substantial additional testing is needed before the development of a generic failure model can be considered.

6.3 The Damage Zone Transition

Little attention has yet been devoted to the transition, at the blunting threshold, between frontal and side lobe damage. Some preliminary considerations of this problem are presented, as a basis for detailed subsequent investigation. An appropriate basis for initiating analysis is to presume that cavity nucleation during crack growth is microstructurally determined and confined to that facet contiguous with

the crack tip.* Conversely, side-lobe damage may be considered to initiate in response to the continuum crack tip field. Hence, a tentative criterion for damage zone initiation may be predicated on the prerequisite that the shear displacement exceed some critical value; a criterion suggested by observations of cavity nucleation during creep [20]. Analysis of the shear displacement on these notions, provides some insight concerning the transition.

The continuum displacement field in a linearly viscous solid has the form

$$\dot{w} \sim K\sqrt{r}/\eta \tag{4}$$

where $\dot{w}$ is the displacement rate and r is the distance from the crack tip. Continuum damage initiates when the sliding displacement reaches a critical value, w_c. In order to initiate side-lobe damage the sliding displacement on a facet a distance, l (facet length), beside the crack tip must satisfy,

$$\xi K\sqrt{l}\Delta t/\eta \geq w_c \tag{5}$$

where Δt is the waiting time between crack growth increments and ξ is a constant. Noting that, $\Delta t = l/\dot{a}$ and that $\dot{a}$ is given by Eq. (2), the crack growth threshold condition becomes;

$$(K_{th}/K_c)^{n-1} = \xi K_c l^{3/2}\exp(Q/RT)/w_c\dot{a}_o \tag{6}$$

Furthermore, since the activation energies for crack growth and viscous flow are generally similar, the relation

$$\eta = \eta_o\exp[Q/RT] \tag{7}$$

where η_o is temperature independent, can be used to simplify Eq. (6), to;

$$\frac{K_{th}}{K_c} = \left[\frac{\xi K_c l^{3/2}}{w_c \dot{a}_o \eta_o}\right]^{1/(n-1)} \tag{8}$$

This result suggests that K_{th}/K_c is temperature independent, consistent with preliminary measurements (Fig. 6a). Furthermore, K_{th}/K_c is anticipated to increase with an increase in grain size; however, data to assess this prediction are not yet available.

*Cavity nucleation on this facet could, for example, be initiated by a sliding transient induced during a prior crack advance increment.

7.—CONCLUDING REMARKS

The process of high temperature failure is of sufficient complexity, involving stages of crack nucleation, growth, blunting and coalescence, that simple models are deemed unlikely to be of general merit. However, progress toward definition of the important stages of failure and the development of preliminary models for each process provides encouragement that continued research is capable of generating the requisite models. The research must devote equal attention to the acquisition of data and the development of models. In addition to failure time data, measurements of the crack nucleation probability and its dependence on the distribution of heterogeneities would be most revealing. Further studies of the coalescence of blunted extrinsic cracks along shear bands are also considered to be a high priority, as well as experiments that allow interpretation of the damage zone transition at the-blunting threshold.

REFERENCES

1. JOHNSON, S.M., BLUMENTHAL, W. and EVANS, A.G., J. Am. Ceram. Soc., in press.
2. BLUMENTHAL, W. and EVANS, A.G., J. Am. Ceram. Soc., in press.
3. DALGLEISH, B.J., JOHNSON, S.M., BLUMENTHAL, W. and EVANS, A.G., J. Am. Ceram. Soc., in press.
4. WALLES, K.F.A., Proc. Brit. Ceram. Soc. 15 (1972) 157.
5. CHARLES, R.J., "Fracture Mechanics of Ceramics," (eds. R.C. Bradt, F.F. Lange, D.P.H. Hasselman) Plenum, N. Y. (1978), vol. 4, p. 623.
6. TRANTINA, G.G. and JOHNSON, C.A., J. Am. Ceram. Soc. 58 (1975) 344.
7. DALGLEISH, B.J. and EVANS, A.G., J. Am. Ceram. Soc., in press.
8. EVANS, A.G. J. Am. Ceram. Soc. 65 (1982) 497.
9. LANGE, F.F., J. Am. Ceram. Soc. 66 (1983) 398.
10. RITTER, J.E., WIEDERHORN, S.M., TIGHE, N.J. and FULLER, E.R., Ceramics for High Performance Applications (Ed. E.M. Lenoe, R.N. Katz) Plenum, N. Y., vol. 6, p. 503.
11. WIEDERHORN, S.M. and TIGHE, N.J., J. Mat. Sci. 13 (1978) 1781.
12. LANGE, F.F., J. Am. Ceram. Soc. 61 (1978) 270.
13. EVANS, A.G., Acta Met. 26 (1978) 1845.
14. LEWIS, M.H., KARUNARATNE, B.S.B., MEREDITH, J. and PICKERING, C., "Creep and Fracture of Engineering Materials and Structures" (Eds. B. Wilshire and D.R.J. Owens), Pineridge, U.K. (1981) 365.
15. THOULESS, M.D., HSEUH, C.H. and EVANS, A.G., Acta Met., in press.
16. MARION, J., DRORY, M.D., EVANS, A.G. and CLARKE, D.R., Acta Met., in press.
17. ARGON, A.S., Scripta Met. 17 (1983) 5.
18. HUTCHINSON, J.W., Acta Met., in press.
19. DAVIES, R., this volume.
20. FLECK, R.G., TAPLIN, D.M.R., BEEVERS, C.J., Acta Met. 23 (1975) 415.
21. RICE, J.R., Acta Met. 29 (1981) 675.
22. HSEUH, C.H. and EVANS, A.G., Acta Met. 29 (1981) 1907.
23. EVANS, A.G. and RANA, A., Acta Met. 28 (1980) 129.
24. McCLINTOCH, F.A., "Fracture Mechanics of Ceramics," (Eds. R.C. Bradt, F.F. Lange, and D.P.H. Hasselman) Plenum, N. Y. (1974), vol. 1, p. 93.

APPENDIX

Some Models of Failure

Crack Nucleation. The nucleation of cracks generally occurs by the coalescence of cavities growing by diffusion. The cavity growth rate is usually limited by the viscous relaxation of the dilatation occurring in the damage zone. Consequently, the coalescence time depends principally on the creep rate of the material and the creep mechanism. For a power law creeping material, creep within the grain results in an elongated cavitated zone and a nucleation time [21],

$$t_c \dot{\varepsilon}_\infty = (2/3)(\lambda/l)\text{cosec}\,[1/(1+\cos\phi) - (\cos\phi)/2] \qquad (A1)$$

where ϕ is the dihedral angle. In material subject to diffusional creep, and a low grain boundary viscosity, the cavitation is subject to a larger constraint and the nucleation time is given by [22];

$$t_c \dot{\varepsilon} \approx 50\,(\lambda_s/\sigma l)^{1/2}\sin(\phi/4)^{3/2}(D_s\delta_s/D_b\delta_b)^{1/2} \qquad (A2)$$

where γ_s is the surface energy, $D_s\delta_s$ is the surface diffusion parameter and $D_b\delta_b$ is the grain boundary diffusion parameter.

In both cases, the product $t_c\dot{\varepsilon}_\infty$ is essentially stress independent and thus at variance with the substantial stress dependence of the failure time.

Macrocrack Propagation. The growth time for macrocracks can be obtained by invoking the stress intensity relation for a semicircular surface crack,

$$K = (2/\pi)\sigma\sqrt{a} \quad . \qquad (A3)$$

Then, from Eq. (2), we obtain,

$$da/a^{n/2} = (2\,\sigma/\pi K_c)\,\dot{a}_o e^{-Q/RT}\,dt \qquad (A4)$$

Integration of Eq. (A4) gives a macrocrack propagation time,

$$t_p = \left(\frac{K_c}{2\sigma}\right)^n \frac{2\exp(Q/RT)}{(n-2)\dot{a}_o}\left[\frac{1}{a_*^{(n-2)/2}} - \frac{1}{a_c^{(n-2)/2}}\right] \qquad (A5)$$

where a_* is the initial size of the macrocrack and a_c is the critical size. For failure from a pre-existing crack of initial size, a_*, Eq. (A5) clearly gives the dependence, $t_p \sim \sigma^{-n}$. Some failure data obtained at high stresses and intermediate temperatures may be explained by this

relation [6]. However, at higher temperatures and longer times when macrocracks form by the coalescence of several small intrinsic cracks, it seems more pertinent to allow the macrocrack to initiate growth at K_{th}, whereupon;

$$a^* = (\pi K_{th}/2\sigma)^2 \quad . \tag{A6}$$

Then, the propagation time becomes;

$$t_p = \frac{2\ \exp(Q/RT)}{(n-2)\ \dot{a}_o} \left(\frac{\pi K_c}{2\sigma}\right)^2 \left[\left(\frac{K_c}{K_{th}}\right)^{n-2} - 1\right] \tag{A7}$$

Consequently, the relation, $t_p \sim \sigma^{-2}$, invariably pertains. Again, this level of stress dependence is at variance with the failure time data.

Crack Coalescence. When cracks nucleate and grow to their arrest size in a fully independent manner, i.e., no interaction effects are allowed, a relatively straightforward probabilistic treatment of failure can be adopted [23,24]. In particular, a probabilistic distribution of times, t_a, required for cracks to attain their arrest dimensions may firstly be assumed,

$$p = (t_a/t_o)^k \tag{A8}$$

where p is the cumulative probability of observing a blunted intrinsic crack in unit volume of material at time t_a, k is the shape parameter and t_o is the scale parameter.* Furthermore, if it is assumed that the joining of blunted cracks across the intervening shear bands is not rate limiting, macrocrack formation depends on the probability of forming sufficient contiguous intrinsic cracks to create a macrocrack of size, a*. Then, it can be readily shown that the failure time at the median probability level varies as [23];

$$\ln t_f = \ln t_o - \left(\frac{4\sigma^2 c_*}{\pi k\ K_{th}^2}\right) \ln\ (4A/c_*^2) \tag{A9}$$

where c* is the length of the blunted intrinsic cracks and A is the area of specimen subject to the stress, σ. The time t_o has a stress dependence characteristic of the intrinsic crack nucleation and growth process. However, even if this

*The arrest time includes a time for nucleation, as well as a growth time for the intrinsic cracks. No assumption is required regarding the more time consuming of these two processes.

process is essentially linear (as would probably obtain if the arrest sequence were nucleation limited, (Eqs. (A1,A2)), then the failure time is still nonlinear, due to the effect of stress on the crack size at the threshold, K_{th} (the second term on the right hand side of Eq. (A9)).

The primary limitation of the model is the requirement that crack linkage across the shear band occur readily, and that failure is dominated by the crack formation probability. There is, as yet, no evidence to support this premise. In fact, observations (Fig. 1d) indicate that the linkage across shear bands may be the limiting process, whereupon Eq. (A9) would not apply.

This report was done with support from the Department of Energy. Any conclusions or opinions expressed in this report represent solely those of the author(s) and not necessarily those of The Regents of the University of California, the Lawrence Berkeley Laboratory or the Department of Energy.

Reference to a company or product name does not imply approval or recommendation of the product by the University of California or the U.S. Department of Energy to the exclusion of others that may be suitable.

TECHNICAL INFORMATION DEPARTMENT
LAWRENCE BERKELEY LABORATORY
UNIVERSITY OF CALIFORNIA
BERKELEY, CALIFORNIA 94720